Search for bosonic super-WIMP interactions with the XENON100 experiment

Aprile, E.; Aalbers, J.; Breur, P.A.; Brown, A.; Colijn, A.P.; Decowski, M.P.; Tiseni, A.; XENON Collaboration

DOI
10.1103/PhysRevD.96.122002

Publication date
2017

Document Version
Final published version

Published in
Physical Review D. Particles, Fields, Gravitation, and Cosmology

PHYSICAL REVIEW D **96,** 122002 (2017)

Search for bosonic super-WIMP interactions with the XENON100 experiment

E. Aprile,[1] J. Aalbers,[2] F. Agostini,[3,4] M. Alfonsi,[5] L. Althueser,[6] F. D. Amaro,[7] M. Anthony,[1] F. Arneodo,[8] P. Barrow,[9] L. Baudis,[9,*] B. Bauermeister,[10] M. L. Benabderrahmane,[8] T. Berger,[11] P. A. Breur,[2] A. Brown,[2] A. Brown,[9] E. Brown,[11] S. Bruenner,[12] G. Bruno,[3] R. Budnik,[13] L. Bütikofer,[14,†] J. Calvén,[10] C. Capelli,[9] J. M. R. Cardoso,[7] D. Cichon,[12] D. Coderre,[14] A. P. Colijn,[2] J. Conrad,[10] J. P. Cussonneau,[15] M. P. Decowski,[2] P. de Perio,[1] P. Di Gangi,[4] A. Di Giovanni,[8] S. Diglio,[15] G. Eurin,[12] J. Fei,[16] A. D. Ferella,[10] A. Fieguth,[6] W. Fulgione,[3,17] A. Gallo Rosso,[3] M. Galloway,[9] F. Gao,[1] M. Garbini,[4] C. Geis,[5] L. W. Goetzke,[1] Z. Greene,[1] C. Grignon,[5] C. Hasterok,[12] E. Hogenbirk,[2] J. Howlett,[1] R. Itay,[13] B. Kaminsky,[14,†] S. Kazama,[9,‡] G. Kessler,[9] A. Kish,[9] H. Landsman,[13] R. F. Lang,[18] D. Lellouch,[13] L. Levinson,[13] Q. Lin,[1] S. Lindemann,[14] M. Lindner,[12] F. Lombardi,[16] J. A. M. Lopes,[7,§] A. Manfredini,[13] I. Maris,[8] T. Marrodán Undagoitia,[12] J. Masbou,[15] F. V. Massoli,[4] D. Masson,[18] D. Mayani,[9] M. Messina,[8,1] K. Micheneau,[15] A. Molinario,[3] K. Morå,[10] M. Murra,[6] J. Naganoma,[19] K. Ni,[16] U. Oberlack,[5] P. Pakarha,[9] B. Pelssers,[10] R. Persiani,[15] F. Piastra,[9] J. Pienaar,[18] V. Pizzella,[12] M.-C. Piro,[11] G. Plante,[1] N. Priel,[13] D. Ramírez García,[14] L. Rauch,[12] S. Reichard,[9,18] C. Reuter,[18] A. Rizzo,[1] N. Rupp,[12] J. M. F. dos Santos,[7] G. Sartorelli,[4] M. Scheibelhut,[5] S. Schindler,[5] J. Schreiner,[12] M. Schumann,[14] L. Scotto Lavina,[20] M. Selvi,[4] P. Shagin,[19] M. Silva,[7] H. Simgen,[12] M. v. Sivers,[14,†] A. Stein,[21] D. Thers,[15] A. Tiseni,[2] G. Trinchero,[17] C. Tunnell,[22] M. Vargas,[6] H. Wang,[21] Z. Wang,[3] Y. Wei,[16,9] C. Weinheimer,[6] C. Wittweg,[6] J. Wulf,[9] J. Ye,[16] Y. Zhang,[1] and T. Zhu[1]

(XENON Collaboration)[‖]

[1]*Physics Department, Columbia University, New York, New York 10027, USA*
[2]*Nikhef and the University of Amsterdam, Science Park, 1098XG Amsterdam, Netherlands*
[3]*INFN-Laboratori Nazionali del Gran Sasso and Gran Sasso Science Institute, 67100 L'Aquila, Italy*
[4]*Department of Physics and Astrophysics, University of Bologna and INFN-Bologna, 40126 Bologna, Italy*
[5]*Institut für Physik & Exzellenzcluster PRISMA, Johannes Gutenberg-Universität Mainz, 55099 Mainz, Germany*
[6]*Institut für Kernphysik, Westfälische Wilhelms-Universität Münster, 48149 Münster, Germany*
[7]*LIBPhys, Department of Physics, University of Coimbra, 3004-516 Coimbra, Portugal*
[8]*New York University Abu Dhabi, P.O. Box 129188, Abu Dhabi, United Arab Emirates*
[9]*Physik-Institut, University of Zurich, 8057 Zurich, Switzerland*
[10]*Oskar Klein Centre, Department of Physics, Stockholm University, AlbaNova, Stockholm SE-10691, Sweden*
[11]*Department of Physics, Applied Physics and Astronomy, Rensselaer Polytechnic Institute, Troy, New York 12180, USA*
[12]*Max-Planck-Institut für Kernphysik, 69117 Heidelberg, Germany*
[13]*Department of Particle Physics and Astrophysics, Weizmann Institute of Science, Rehovot 7610001, Israel*
[14]*Physikalisches Institut, Universität Freiburg, 79104 Freiburg, Germany*
[15]*SUBATECH, IMT Atlantique, CNRS/IN2P3, Université de Nantes, Nantes 44307, France*
[16]*Department of Physics, University of California, San Diego, California 92093, USA*
[17]*INFN-Torino and Osservatorio Astrofisico di Torino, 10125 Torino, Italy*
[18]*Department of Physics and Astronomy, Purdue University, West Lafayette, Indiana 47907, USA*
[19]*Department of Physics and Astronomy, Rice University, Houston, Texas 77005, USA*
[20]*LPNHE, Université Pierre et Marie Curie, Université Paris Diderot, CNRS/IN2P3, Paris 75252, France*
[21]*Physics & Astronomy Department, University of California, Los Angeles, California 90095, USA*
[22]*Department of Physics & Kavli Institute of Cosmological Physics, University of Chicago, Chicago, Illinois 60637, USA*

(Received 8 September 2017; published 7 December 2017)

We present results of searches for vector and pseudoscalar bosonic super-weakly interacting massive particles (WIMPs), which are dark matter candidates with masses at the keV-scale, with the XENON100

[*]laura.baudis@uzh.ch
[†]Also at Albert Einstein Center for Fundamental Physics, University of Bern, 3012 Bern, Switzerland.
[‡]kazama@physik.uzh.ch
[§]Also at Coimbra Engineering Institute, Coimbra, Portugal.
[‖]xenon@lngs.infn.it

2470-0010/2017/96(12)/122002(6)

experiment. XENON100 is a dual-phase xenon time projection chamber operated at the Laboratori Nazionali del Gran Sasso. A profile likelihood analysis of data with an exposure of 224.6 live days ×34 kg showed no evidence for a signal above the expected background. We thus obtain new and stringent upper limits in the (8–125) $\mathrm{keV/c^2}$ mass range, excluding couplings to electrons with coupling constants of $g_{ae} > 3 \times 10^{-13}$ for pseudo-scalar and $\alpha'/\alpha > 2 \times 10^{-28}$ for vector super-WIMPs, respectively. These limits are derived under the assumption that super-WIMPs constitute all of the dark matter in our galaxy.

DOI: 10.1103/PhysRevD.96.122002

I. INTRODUCTION

There is overwhelming evidence for the presence of dark matter in our universe. Its existence is inferred from a variety of observations, including those of the temperature fluctuations in the cosmic microwave background [1], gravitational lensing [2], mass-to-light ratio in galaxy clusters [3], and galactic rotation curves [4]. In addition, simulations of large-scale structure and galaxy formation require the presence of nonbaryonic matter to reproduce the observed cosmic structures [5].

While the microscopic nature of dark matter is largely unknown, the simplest assumption which can explain all existing observations is that it is made of a new, as yet undiscovered particle [6]. Leading examples are weakly interacting massive particles (WIMPs), axions or axionlike-particles (ALPs) and sterile neutrinos. WIMPs with masses in the GeV range, as well as axions/ALPs are examples for cold dark matter (CDM), while sterile neutrinos with masses at the keV-scale are an example for warm dark matter (WDM). While CDM particles were nonrelativistic at the time of their decoupling from the rest of the particles in the early universe, WDM particles remain relativistic for longer, retaining a larger velocity dispersion and more easily free-streaming out from small-scale perturbations. Astrophysical and cosmological observations constrain the mass of WDM to be larger than $\sim 3\ \mathrm{keV/c^2}$ [7,8], with a more recent lower limit from Lyman-α forest data being 5.3 keV [9].

A large number of experiments aim to observe axions/ALPs and WIMPs: directly, indirectly, or via production at the LHC [10]. Direct detection experiments, which look for low energy nuclear recoils produced in collisions of WIMPs with atomic nuclei feature low energy thresholds, large detector masses and ultralow backgrounds [11,12]. Such experiments can thus also observe other type of particles, with nonvanishing couplings to electrons. Among these, bosonic super-WIMPs [13] are an example for WDM. These particles, with masses at the keV-scale, could couple electromagnetically to standard model particles via the axioelectric effect, which is an analogous process to the photoelectric effect, and thus be detected in direct detection experiments [13].

In this study we present a search for vector and pseudo-scalar bosonic super-WIMPs with the XENON100 detector. The super-WIMPs can be absorbed in liquid xenon (LXe) and the expected signature is a monoenergetic peak at the super-WIMP's rest mass. We have presented first results on pseudoscalar bosonic super-WIMPs, or axionlike particles, in Ref. [14]. In this analysis we include two major improvements: we extend the mass range up to 125 $\mathrm{keV/c^2}$ and we improve the energy resolution by employing both scintillation and ionization signals to determine the energy scale and resolution of the XENON100 detector.

This paper is organized as follows. We describe the main features of the XENON100 experiment in Sec. II, after which we briefly review the expected signal and rates in a dark matter detector in Sec. III. We detail the data analysis methods in Sec. IV and present our main findings in Sec. V, together with a discussion of their implications.

II. THE XENON100 DETECTOR

Located at the Laboratori Nazionali del Gran Sasso (LNGS), the XENON100 experiment operates a dual-phase (liquid and gas) xenon time projection chamber (TPC). The detector contains 161 kg of LXe in total, with 62 kg in the active region of the TPC. A total of 178 1-inch square, low-radioactivity, UV-sensitive photomultiplier tubes (PMTs) arranged in two arrays, one in the liquid and one in the gas, detect the prompt scintillation (S1) and the delayed, proportional scintillation signal (S2) arising when a particle interacts in the TPC. The ionisation electrons are drifted via an electric field of 530 V/cm to the liquid-gas boundary and extracted in the vapour phase via a ~ 12 kV/cm field, where proportional scintillation is produced. The three-dimensional position of the original interaction site is reconstructed via the time difference between the S1 and S2 signal (z-position, with a 1σ resolution < 0.3 mm), and by exploiting the S2 light pattern in the top PMT array ((x, y)-position, with a 1σ resolution < 3 mm). This enables us to reject a large fraction of background events via fiducial volume cuts and selection of single-scatters [15]. A 4 cm thick, 99 kg LXe, layer surrounds the TPC and is observed by 64 1-inch square PMTs, allowing us to rejects events with energy depositions in this active LXe region. Finally, nuclear recoils (NRs) induced by fast neutrons and WIMP-nucleus scatters, and electronic recoils (ERs), produced by β and γ-rays, as well as axions, can be distinguished based on their (S2/S1)-ratio.

The XENON100 experiment is described in detail in [15]. In this analysis, we use the Run II science data, with

224.6 live days of data taking and 34 kg of LXe in the fiducial region, to search for signatures from bosonic super-WIMPs in the mass range (8–125) $\mathrm{keV/c^2}$ in the ER spectrum. A previous search in LXe was conducted by XMASS, constraining the mass range (40–120) $\mathrm{keV/c^2}$ [16], and recent searches for axions/ALPs were conducted by LUX [17] and PandaX-II [18].

III. EXPECTED SIGNAL

Viable models for super-WIMPs as dark matter candidates result in vector and pseudoscalar particles [13]. The expected interaction rates in a detector are obtained by convoluting the absorption cross section with the expected flux of these particles. The absorption cross section σ_{abs} for vector super-WIMPs can be written in terms of the cross section for photon absorption via the photoelectric effect σ_{pe}, with the photon energy ω replaced by the mass of the vector boson m_v:

$$\frac{\sigma_{abs} v}{\sigma_{pe}(\omega = m_v)c} \simeq \frac{\alpha'}{\alpha}, \tag{1}$$

where v is the incoming velocity of the vector boson, c is the velocity of light, α and α' are the fine structure constant, and its vector boson equivalent, respectively.

For pseudoscalar super-WIMPs, the relation between the two cross sections is as follows:

$$\frac{\sigma_{abs} v}{\sigma_{pe}(\omega = m_a)c} \simeq \frac{3m_a^2}{4\pi\alpha f_a^2}, \tag{2}$$

where m_a is the mass of the pseudoscalar particle, and f_a is a dimensional coupling constant.

Assuming that super-WIMPs are nonrelativistic, and that their local density is 0.3 $\mathrm{GeV/cm^3}$ [19], the interaction rate in a direct detection experiment can be expressed as [13]:

$$R \simeq \frac{4\times 10^{23}}{A}\frac{\alpha'}{\alpha}\left(\frac{\mathrm{keV}}{m_v}\right)\left(\frac{\sigma_{pe}}{\mathrm{b}}\right)\ \mathrm{kg^{-1}\,d^{-1}}, \tag{3}$$

and

$$R \simeq \frac{1.29\times 10^{19}}{A} g_{ae}^2\left(\frac{m_a}{\mathrm{keV}}\right)\left(\frac{\sigma_{pe}}{\mathrm{b}}\right)\ \mathrm{kg^{-1}\,d^{-1}}, \tag{4}$$

for vector and pseudoscalar super-WIMPs, respectively. $g_{ae} = 2m_e f_a^{-1}$ is the axioelectric coupling, m_e is the mass of the electron, and A is the atomic number of the target atom.

With Eqs. (3) and (4), we can predict the interaction rate in XENON100, assuming a range of coupling constants, and an exposure of 34 kg × 224.6 live days, as shown in Figs. 1 and 2 for vector and pseudoscalar super-WIMPs, respectively. The structures observed around 35 keV, as well as at lower energies are due to an increase in the cross section of the photoelectric effect in xenon at these energies, when new atomic energy levels are excited [20].

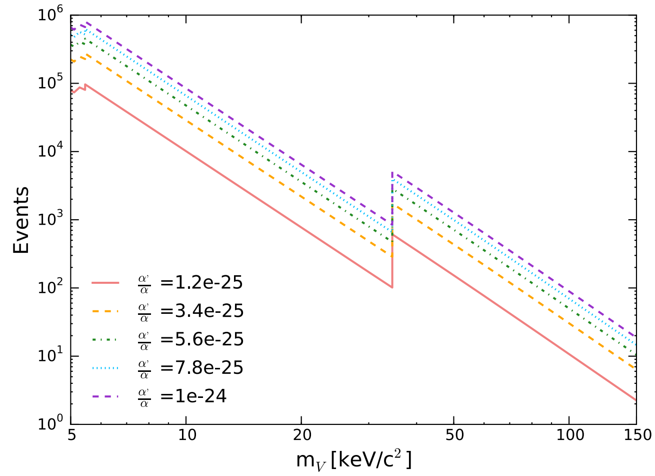

FIG. 1. Predicted total number of events, assuming an infinite energy resolution, for vector super-WIMPs in XENON100 as a function of mass for a range of coupling constants. The assumed exposure is 34 kg × 225 live days of data.

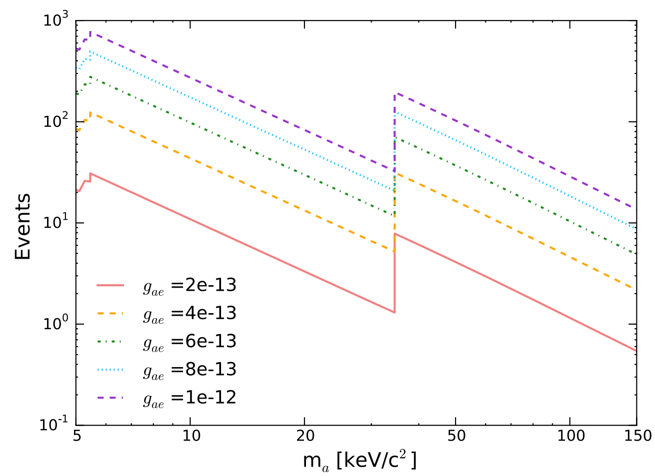

FIG. 2. Predicted total number of events, assuming an infinite energy resolution, for pseudoscalar super-WIMPs in XENON100 as a function of mass for a range of coupling constants. The assumed exposure is 34 kg × 225 live days of data.

IV. DATA ANALYSIS

We perform this analysis using XENON100 Run II science data, with 224.6 live days of data and 34 kg of LXe in the fiducial region. Our data selection and treatment is similar to the one described in [14], with a few differences, to be detailed below. In particular, this is the first analysis of the XENON100 electronic recoil data that extends up to an energy of 140 keV. The overall background in the low-energy region is 5.3×10^{-3} events/(kg d keV) and it is flat in shape, because it is dominated by Compton scatters of high-energy gammas originating from the radio-activity of detector materials [21].

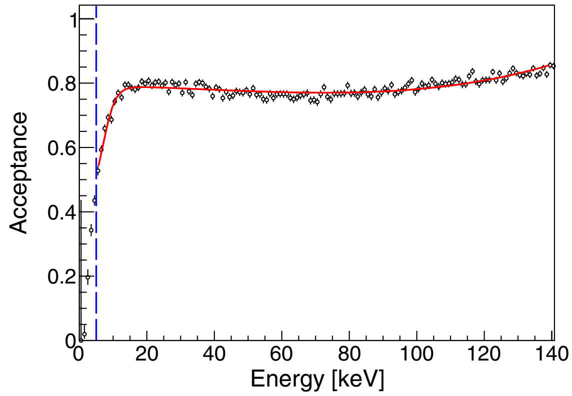

FIG. 3. Calculated acceptance ϵ to electronic recoils (black dots) of all the event selection criteria as a function of energy, along with a fit (red curve) to the distribution. The energy threshold employed in this analysis (5 keV) is shown by the vertical dashed line.

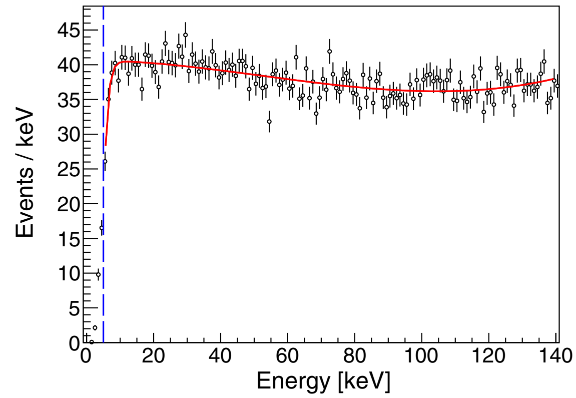

FIG. 4. Background model $N_b \times f_b$ (red line) scaled to the correct exposure. The model is based on ^{60}Co and ^{232}Th calibration data (black dots) and used in Eq. (5). The energy threshold of 5 keV is shown by the vertical dashed line.

A. Event selection and signal region

An interaction in the LXe-TPC gives rise to an S1 and a correlated S2 signal with a certain number of photoelectrons (PE) observed by the photosensors. To select valid events, we apply event selection criteria as described in [14]. These include basic data quality selection criteria, single-scatter and fiducial volume selection, and signal consistency checks. Furthermore, we use position-corrected S1 and S2 quantities as detailed in [15,22]. In contrast with [14], we determine the energy deposition of an interaction in LXe by using a linear combination of the prompt and delayed scintillation light signals, where we employ the S2 signal detected by the bottom PMT arrays only ($S2_b$), due to smaller required corrections. This energy scale improves our energy resolution (at 1-σ) from 14%, based on S1-only, to 5.7% at an energy of ∼100 keV [15].

The combined acceptance of all applied event selection criteria, evaluated on calibration data acquired with ^{60}Co and ^{232}Th sources, is shown in Fig. 3. This acceptance, around 80%, is rather flat in energy above ∼15 keV, below which it decreases to reach 53% at 5 keV.

The background events in the region of interest are predominantly due to interactions of γ-rays from decays of radioactive isotopes in the detector materials, yielding low-energy Compton-scatters, and from β-decays of the ^{222}Rn and ^{85}Kr isotopes distributed in the liquid xenon [21]. To model the expected shape of the background distribution in the region of interest, we employ calibration data acquired with ^{60}Co and ^{232}Th sources. The spectral shape is parameterised with a modified Fermi function, as shown in Fig. 4, together with the calibration data.

B. Statistical method

A profile likelihood analysis is employed to constrain the coupling constants g_{ae} and α'/α, as described in [23,24]. The full likelihood function is given by

$$\mathcal{L}((g_{ae}, \alpha'/\alpha), N_b) = \mathrm{Poiss}(N|N_s + N_b) \prod_{i=1}^{N} \frac{N_s f_s(E_i) + N_b f_b(E_i)}{N_s + N_b}, \quad (5)$$

where the parameters of interest are g_{ae} or α'/α and N_b and N_s are the expected number of background and signal events in the search region, respectively. N_b is considered as nuisance parameter, N_s is a function of the coupling constant, and the functions f_b and f_s are the background and signal probability distribution functions. N is the total number of observed events and E_i corresponds to the energy of the ith event. We model the expected event rate at a given energy with a Gaussian smeared with the energy resolution of the detector and multiplied by the total acceptance of the data selection criteria, shown in Fig. 3.

Our selected region of interest extends from 5 keV to 140 keV. The lower bound is chosen such as to have > 50% acceptance of the data selection criteria, as mentioned above. The upper bound is given by the width of the 164 keV line from ^{131m}Xe decays, present in both calibration and physics data due to the activation of xenon during an AmBe neutron calibration. The relative resolution at this energy is 4.6%, and we consider the region up to 3-σ to the left of the peak.

For each considered mass m_a of the bosonic super-WIMP, the ±2-σ-region, as determined by the energy resolution at the given energy, is blinded. The number of events outside of this region is then used to scale the background model f_b shown in Fig. 4, and thus to predict the number of expected background events in the signal region. Since the ±2-σ window must not exceed the search region between (5–140) keV, the range of bosonic super-WIMP masses is restricted to (8–125) keV. We use the CL_s prescription [25] to protect against overly constrained parameters due to downward fluctuations in the background.

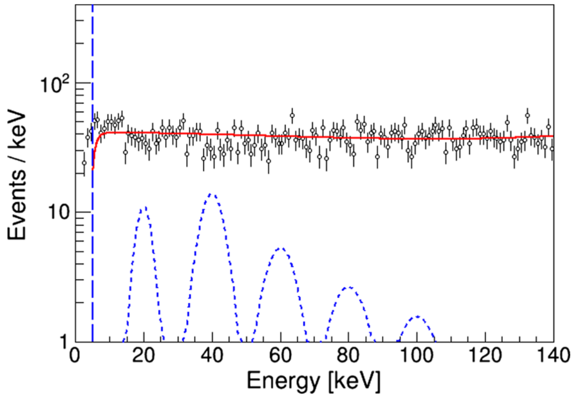

FIG. 5. Distribution of events (black dots with error bars) in the super-WIMP search region between (5–140) keV. The background model (red curve) along with the expected signal for various pseudoscalar super-WIMP masses (20, 40, 60, 80 and 100 keV) and a coupling of $g_{Ae} = 1 \times 10^{-12}$ (blue dashed peaks) is also shown. The vertical dashed line indicated the energy threshold in this analysis.

V. RESULTS

Figure 5 shows the distribution of events in the region of interest, together with the expected signal for different pseudoscalar super-WIMP masses and an assumed coupling of $g_{ae} = 1 \times 10^{-12}$. We also assume that these particles constitute all the dark matter in our galaxy, with a local density of 0.3 $\mathrm{GeV/cm^3}$. The widths of the monoenergetic signals are given by the energy resolution of the detector, in combined energy scale, at the given S1 and $S2_b$ signal size.

Our data are compatible with the background only hypothesis, and no excess above the predicted background is observed.

Figure 6 shows the 90% C.L. exclusion limit for pseudoscalar (top panel) and vector (bottom panel) super-WIMPs. Our 1-σ (2-σ) expected sensitivity is shown by the dark (light) blue bands. The step in sensitivity around 35 $\mathrm{keV/c^2}$ is due to an increase in the photoelectric cross section as new atomic energy levels are excited. We compare these results with those obtained by the XMASS-I [16], LUX [17] and the Majorana Demonstrator [26] experiments. While the XMASS-I constraints are more stringent in the mass region above 50 $\mathrm{keV/c^2}$, our results improve upon these at lower masses, and in particular extend the excluded mass region down to 8 $\mathrm{keV/c^2}$. Our results are comparable to those of the Majorana Demonstrator in the mass range $\sim$(12–32) $\mathrm{keV/c^2}$, but more stringent at higher masses. Finally, LUX presents the most constraining limit at masses of the pseudoscalar particle below 16 $\mathrm{keV/c^2}$.

The observed fluctuations in our limit are caused by statistical fluctuations in the background (see Fig. 5). Due to the expected monoenergetic shape of the signal, the limit is very sensitive to such fluctuations. We have also studied the impact of systematic uncertainties on the analysis. In particular, we have considered the impact of varying the overall event selection acceptance, the energy resolution, as well as the energy scale. The combined effect of all systematic uncertainties changes the final result by around 10%, however this contribution is small compared to our statistical uncertainty that is accounted for in the profile likelihood analysis.

XENON100 thus sets new and stringent upper limits in the (8–125) $\mathrm{keV/c^2}$ mass range. At 90% C.L. it excludes couplings to electrons $g_{ae} > 3 \times 10^{-13}$ for pseudoscalar super-WIMPs and $\alpha'/\alpha > 2 \times 10^{-28}$ for vector super-WIMPs. These limits are derived under the assumption that super-WIMPs constitute all of the galactic dark matter.

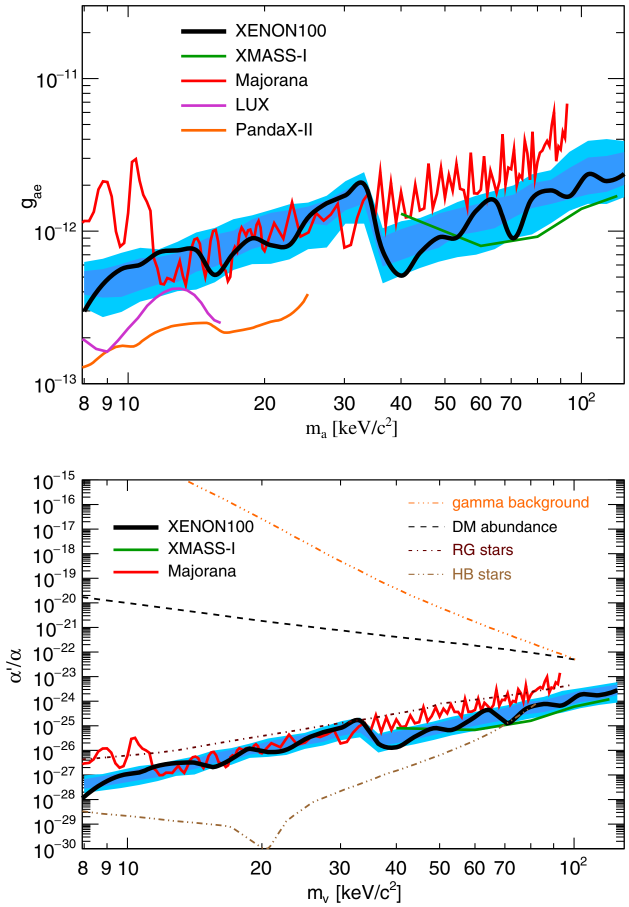

FIG. 6. The XENON100 upper limits, at 90% C.L., on the coupling of pseudoscalar (top) and vector (bottom) super-WIMPs as a function of particle mass. The 1-σ (2-σ) expected sensitivity is shown by the dark (light) blue bands. We compare our limits to the results obtained by the XMASS-I [16] (green), LUX [17] (magenta), PandaX-II [18] (orange) and Majorana Demonstrator [26] (red) experiments, as well as with astrophysical constraints from the gamma background, the dark matter abundance, red giant stars and horizontal branch stars (dashed and dash-dotted) [13] for the case of the vector super-WIMP.

ACKNOWLEDGMENTS

We gratefully acknowledge support from the National Science Foundation, Swiss National Science Foundation, Deutsche Forschungsgemeinschaft, Max Planck Gesellschaft, German Ministry for Education and Research, Netherlands Organisation for Scientific Research, Weizmann Institute of Science, I-CORE, from the European Union's Horizon 2020 research and innovation programme under the Marie Sklodowska-Curie Grant Agreement No. 674896, Fundacao para a Ciencia e a Tecnologia, Region des Pays de la Loire, Knut and Alice Wallenberg Foundation, Kavli Foundation, and Istituto Nazionale di Fisica Nucleare. J. C. is a Wallenberg Academy Fellow. We are grateful to Laboratori Nazionali del Gran Sasso for hosting and supporting the XENON project.

[1] P. A. R. Ade *et al.* (Planck Collaboration), Astron. Astrophys. **571**, A16 (2014).
[2] N. Kaiser and G. Squires, Astrophys. J. **404**, 441 (1993).
[3] F. Zwicky, Helv. Phys. Acta **6**, 110 (1933).
[4] V. C. Rubin and W. K. Ford, Jr., Astrophys. J. **159**, 379 (1970).
[5] C. S. Frenk and S. D. M. White, Ann. Phys. (Berlin) **524**, 507 (2012).
[6] Nat. Phys. **13** (2017).
[7] K. Markovi and M. Viel, Pub. Astron. Soc. Aust. **31**, e006 (2014).
[8] A. Lapi and L. Danese, J. Cosmol. Astropart. Phys. 09 (2015) 003.
[9] V. Irsic *et al.*, Phys. Rev. D **96**, 023522 (2017).
[10] L. Baudis, Ann. Phys. (Berlin) **528**, 74 (2016).
[11] T. M. Undagoitia and L. Rauch, J. Phys. G **43**, 013001 (2016).
[12] L. Baudis, J. Phys. G **43**, 044001 (2016).
[13] M. Pospelov, A. Ritz, and M. B. Voloshin, Phys. Rev. D **78**, 115012 (2008).
[14] E. Aprile *et al.* (XENON100 Collaboration), Phys. Rev. D **90**, 062009 (2014).
[15] E. Aprile *et al.* (XENON100 Collaboration), Astropart. Phys. **35**, 573 (2012).
[16] K. Abe *et al.* (XMASS Collaboration), Phys. Rev. Lett. **113**, 121301 (2014).
[17] D. S. Akerib *et al.* (LUX Collaboration), Phys. Rev. Lett. **118**, 261301 (2017).
[18] C. Fu *et al.* (PandaX Collaboration), Phys. Rev. Lett. **119**, 181806 (2017).
[19] A. M. Green, J. Phys. G **44**, 084001 (2017).
[20] W. J. Veigele, Report No. Print-89-0854, 1973.
[21] E. Aprile *et al.* (XENON100 Collaboration), Phys. Rev. D **83**, 082001 (2011); **85**, 029904(E) (2012).
[22] E. Aprile *et al.* (XENON100 Collaboration), Astropart. Phys. **54**, 11 (2014).
[23] G. Cowan, K. Cranmer, E. Gross, and O. Vitells, Eur. Phys. J. C **71**, 1554 (2011); **73**, 2501(E) (2013).
[24] E. Aprile *et al.* (XENON100 Collaboration), Phys. Rev. D **84**, 052003 (2011).
[25] A. L. Read, in *Workshop on Confidence Limits, CERN, Geneva, Switzerland, 2000: Proceedings* (2000), p. 81, https://cds.cern.ch/record/411537?ln=en.
[26] N. Abgrall *et al.* (Majorana Collaboration), Phys. Rev. Lett. **118**, 161801 (2017).